Supporting information for

"Reduction of the lattice thermal conductivity of polymer semiconductors by molecular doping"

Osnat Zapata-Arteaga,[a] Aleksandr Perevedentsev,[a] Sara Marina,[b] Jaime Martin,[b,c] Juan Sebastián Reparaz,[a*] Mariano Campoy-Quiles.[a*]

[a]Institute of Materials Science of Barcelona (ICMAB-CSIC), Campus of the UAB, 08193, Bellaterra, Spain; E-mail: mcampoy@icmab.es; jsreparaz@icmab.es

[b] POLYMAT and Polymer Science and Technology Department, Faculty of Chemistry, University of the Basque Country UPV/EHU, Manuel de Lardizabal 3, 20018, Donostia- San Sebastián, Spain

[c] Ikerbasque, Basque Foundation for Science, E-48011, Bilbao, Spain

Section I. Materials and Methods

PBTTT-C14 (M_n = 50 kDa; 1-Material), PTB7-Th (Ossila) and F4TCNQ (TCI Chemicals) were used as received. Chlorobenzene (>99%) was purchased from Sigma Aldrich. Polymer films were fabricated from 20 mg/mL solutions in chlorobenzene. Solutions were stirred for 5 h at 110 ºC for both PBTTT and PTB7-Th, and used at these temperatures for deposition. Films were deposited onto conventional 75-mm-long glass slides under nitrogen atmosphere using a pre-heated blade coater (temperatures as above), with a blade height of 200 μm and a speed of 30 mm s^{-1}. These films formed the 'baseline' samples which were then post-processed in two different ways to generate gradients of microstructure and/or doping along the long axis.

In the first case, as-deposited samples were annealed using a temperature gradient (~70–200 ºC) using a Kofler bench for 15 min and then allowed to cool slowly down to room temperature.

In the second case, 'temperature-assisted' vapor doping was performed using the method described in a previous publication[1]. Briefly: PBTTT films were first pre-crystallized by annealing at 180 ºC to avoid simultaneously inducing crystallization during subsequent doping at elevated temperatures. Then ~5 mg of F4TCNQ was placed in the bottom of a reactor beaker and the annealed polymer film fixed to the lid. Then, the bottom of the beaker was heated at 180 ºC while the lid and polymer film were maintained at 130 ºC for a period of 10 min at a reduced pressure (prior heating, and closing all the beaker inlets). Having obtained homogenous, maximally doped samples, doping gradients were then generated via thermally-induced dedoping: that is, by placing the polymer film on a Kofler bench with the temperature range spanning 130–200 ºC for a period of 4 h.

All thermal treatments were performed under nitrogen atmosphere inside a glove box.

Section II. Characterization

Vis-NIR absorption spectra were measured using a Bruker HYPERION FTIR microscope coupled to a VERTEX 70 spectrometer. All measurements were done in a glass and on the same samples described in the main text.

Grazing incidence wide angle X-ray scattering (GIWAXS) analysis was conducted at the BL11 NCD-SWEET beamline at ALBA Synchrotron Radiation Facility (Spain). Samples were illuminated for 5 s with an X-ray beam of 12.4 keV at an angle of incidence of 0.12º. Scattering patterns were acquired using a Rayonix® LX255-HS detector, which positioned at 200.9 mm far from the samples.

Films used for GIWAXS measurements were deposited onto preheated (at 110 ºC) ~ 1cm x 1cm silicon substrates using a spin coater at 1000 rpms for 15 sec, followed by 3000 rpms for 45 sec. The films were cooled to room temperature and post-processed according to the conditions depicted in the main text (Figure 2). 1) as-deposited without annealing and without doping. 2) annealing at 100ºC for 15 min without doping (T_{an} 100ºC). 3) annealing at 180ºC for 15 min without doping (T_{an} 180ºC). 4) Annealing at 180ºC for 15 min and doping using the 'temperature assisted' vapor doping (T_{an} 180ºC + doped) and, 5) dedoped - annealing at 180ºC for 15 min, doping using the 'temperature assisted' vapor doping and dedoping at 180ºC for 4 h.

Thickness of as-deposited films was determined using an Alpha-Step D-500 Stylus Profiler. Typically, differences in thickness of approximately 5–7 % were observed across the length of the glass slide. We consider this effect normal, due to the gradual depletion of polymer solution during film deposition by blade coating.

AFM measurements were done with an AFM Dimension ICON with a Nanoscope V (Bruker) controller. Images were taken in Peak Force tapping mode and employing a ScanAsyst-Air tip from Bruker. Films used for these measurements were fabricated by spin coating a 20 mg / mL solution of PBTTT in chlorobenzene at 2000 rpm for 60 s on silicon substrates.

Section III. Calculation of the electrical conductivity through Raman spectroscopy

Raman scattering mapping was performed with a WITec Alpha 300 RA+ instrument. Continuous-wave laser excitation at 488 nm was used, with both excitation and detection via a 100× objective. Samples were raster scanned in the focal plane of the laser (fast scan axis perpendicular to the long axis of samples and doping gradient direction) using a stepper-motor-driven stage, and a pre-determined topography correction was automatically applied to maintain a consistent focus. Using 80–150 μW excitation laser power and integration time of 0.3 s per single Raman spectrum acquired over a ~1×250 μm^2 area, no appreciable sample degradation (e.g. dedoping) was observed. Following background subtraction and averaging of spectra along the fast scan direction (perpendicular to doping gradient direction), a profile of intensity ratio, r_R, of ~1393 cm^{-1} and 1493 cm^{-1} Raman peaks of PBTTT was extracted. Finally, electrical conductivity σ was estimated from r_R using the empirical relation $r_R = A\sigma^b + C$ ($A = 0.40$, $b = 0.21$, $C = 0.77$ are fit parameters)

determined from 'calibration' measurements of Raman spectroscopy and electrical conductivity performed on similarly processed[1] PBTTT-F4TCNQ films. See also calibration data in Figure S9.

Section IV. Frequency-domain thermoreflectance

Frequency-domain thermoreflectance is a non-destructive contactless optical method that uses two lasers to locally heat (pump, 405 nm) and probe (probe, 532 nm) the local temperature at the surface of a sample.[2] Figure S1 displays a schematic illustration of the experimental setup. In order to enhance the thermal sensitivity of the method and to limit the optical penetration depth, a 65 nm thick Au transducer was evaporated onto the surface of the samples. Both lasers were focused using an achromatic 30 mm focal distance lens to a spot size of ≈10 μm in diameter. The output power of the pump laser was modulated to a harmonic waveform in the frequency range between 1 kHz and 100 kHz, which generates thermally induced harmonic oscillations of the reflectivity of the sample, thus, leading to a modulation of the reflected power of the continuous wave probe laser. The key quantity that we address through this method is the phase lag between the pump heat wave generated by the pump laser, and the harmonic response of the sample as sensed by the probe laser using a lock-in amplifier. The frequency dependent phase lag is modelled numerically solving the parabolic heat equation, Eq. (1), for the described geometry. The thermal model used to fit the phase lag response curve describes the behavior of a stack of layers composed by the Au transducer, the studied film, the substrate, and an effective thermal boundary conductance that accounts for the two interfaces defined between the layers. The cross-plane thermal conductivity ($\kappa_\perp$) and the specific heat capacity (C_p) of the thin films, as well as the effective thermal boundary conductance (G) of the system were fitted using a least-squares routine.

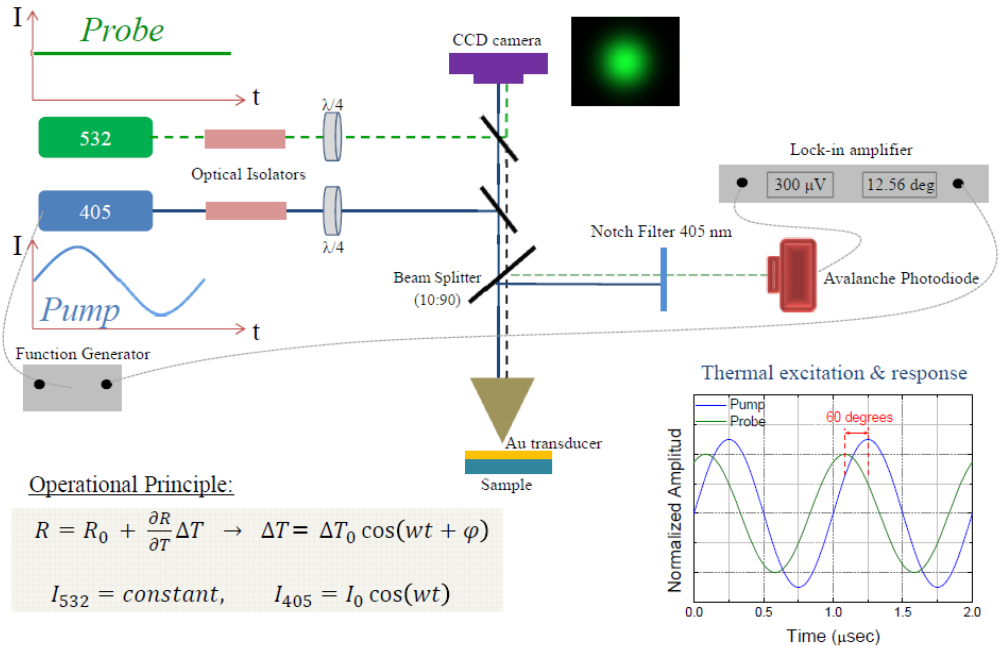

Figure S1: Schematic illustration of the frequency-domain thermoreflectance experimental setup, as well as the operational principle of the technique.

Figure S2 displays a representative phase lag response curve for the case of a 160 nm thick PBTTT thin film. For all measurements we have deposited a 65 nm thick Au transducer through thermal evaporation (base pressure 10^{-6} mbar). The measured data (red full circles) was numerically fitted solving the heat equation in the diffusive approximation:

$$\frac{\kappa}{\rho C_p}\nabla^2 T - \frac{\partial T}{\partial t} = \frac{1}{\rho C_p} S(r,t) \qquad (1)$$

where κ is the thermal conductivity, ρ is the density, C_p is the specific heat, *S(r,t)* is the heat source, and *T* is the temperature. A detailed description of the fitting procedure can be found elsewhere.[2] The previous equation was numerically solved for the multilayer geometry composed by the Au traducer, the PBTTT thin film, and the Glass substrate. Hence, the fitting procedure of the phase lag response in Figure S2 renders the thermal conductivity of each sample. For samples with a lateral variation of a given property, such as microstructure or doping level, we scanned the laser across the sample to obtain the local thermal conductivity (see main text).

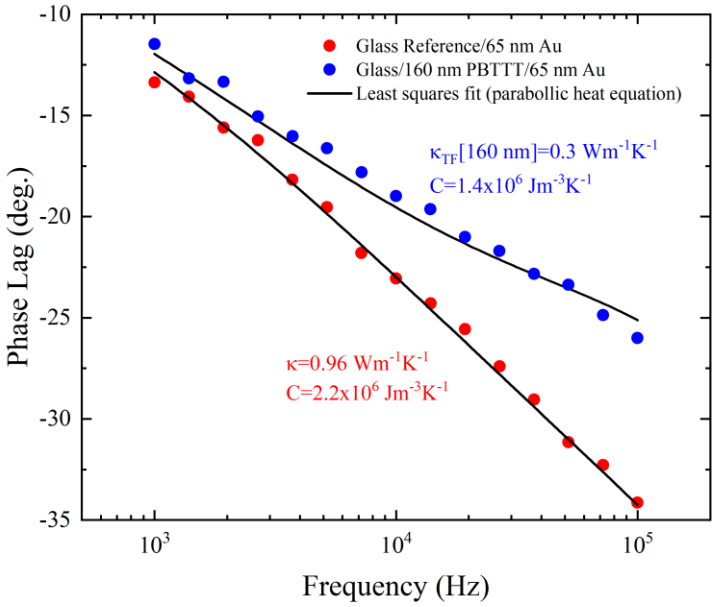

Figure S2: Representative phase lag response curve obtained for the case of a 160 nm thick PBTTT thin (blue full circles). The red full circles represent a reference Glass sample for calibration purposes. The full lines are least squares fits to the data point using equation (1).

Finally, we note that our specific FDTR set up has been further validated with different materials (quartz, silicon wafers) as well as films of PBTTT deposited on silicon using the 3ω technique.

Section V. Estimation of the doping level and exciton band width

We estimate the molar ratio of F4TCNQ anion per PBTTT monomer (MR_D) from the intensity of the F4TCNQ anion and the volume concentration of PBTTT extracted from literature (1.58 mol L^{-1}). In literature, the latter is calculated from the mass of monomer repeating units per unit cell (1 for PBTTT). [3–5]

The absorbance spectra of doped PBTTT was deconvoluted into several Gaussians contributions, for the neutral, anion and polaron species and fitted using a least-square routine implemented in Python (Figure S3b). Then we determined the F4TCNQ anion concentration (C_F) from the intensity of the anion band at 790 for a film of thickness *t,* using an extinction coefficient from literature ($\varepsilon = 50000\ L\ \mathrm{mol}^{-1}\mathrm{cm}^{-1}$ at 790 nm)[5] according to equation 2:

$$C_F = \frac{A}{\varepsilon t} \qquad (2)$$

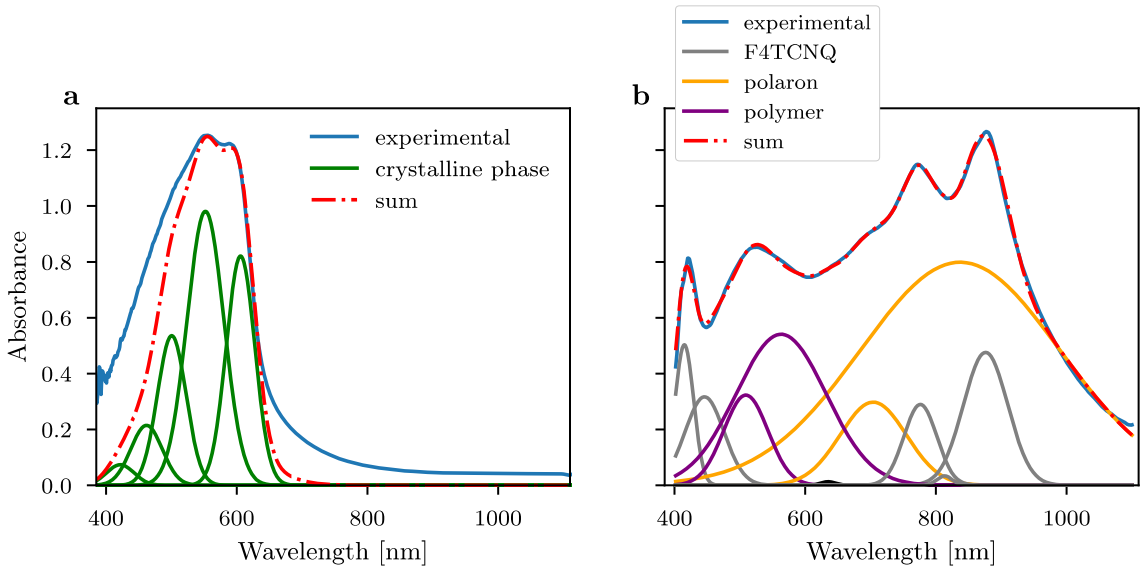

Figure S3: a) Absorption spectra of pristine and b) doped PBTTT. Data shown here was subjected to peak fitting in order to obtain the free exciton bandwidth from a) and the dopant content from b).

The free exciton bandwidth was calculated by evaluating the ratio between the vibronic peaks ascribed to the crystalline phase, $A_{0\text{-}0}$ and $A_{0\text{-}1}$ bands [6,7] according to equation 3:

$$\frac{A_{0-0}}{A_{0-1}} \approx \left(\frac{1-\frac{0.24W}{E_p}}{1+\frac{0.073W}{E_p}} \right)^2 \qquad (3)$$

Where the E_p is the intramolecular vibration of the C=C symmetric stretch ($0.18eV$) and W is the free exciton bandwidth.

Section VI. Additional experimental data

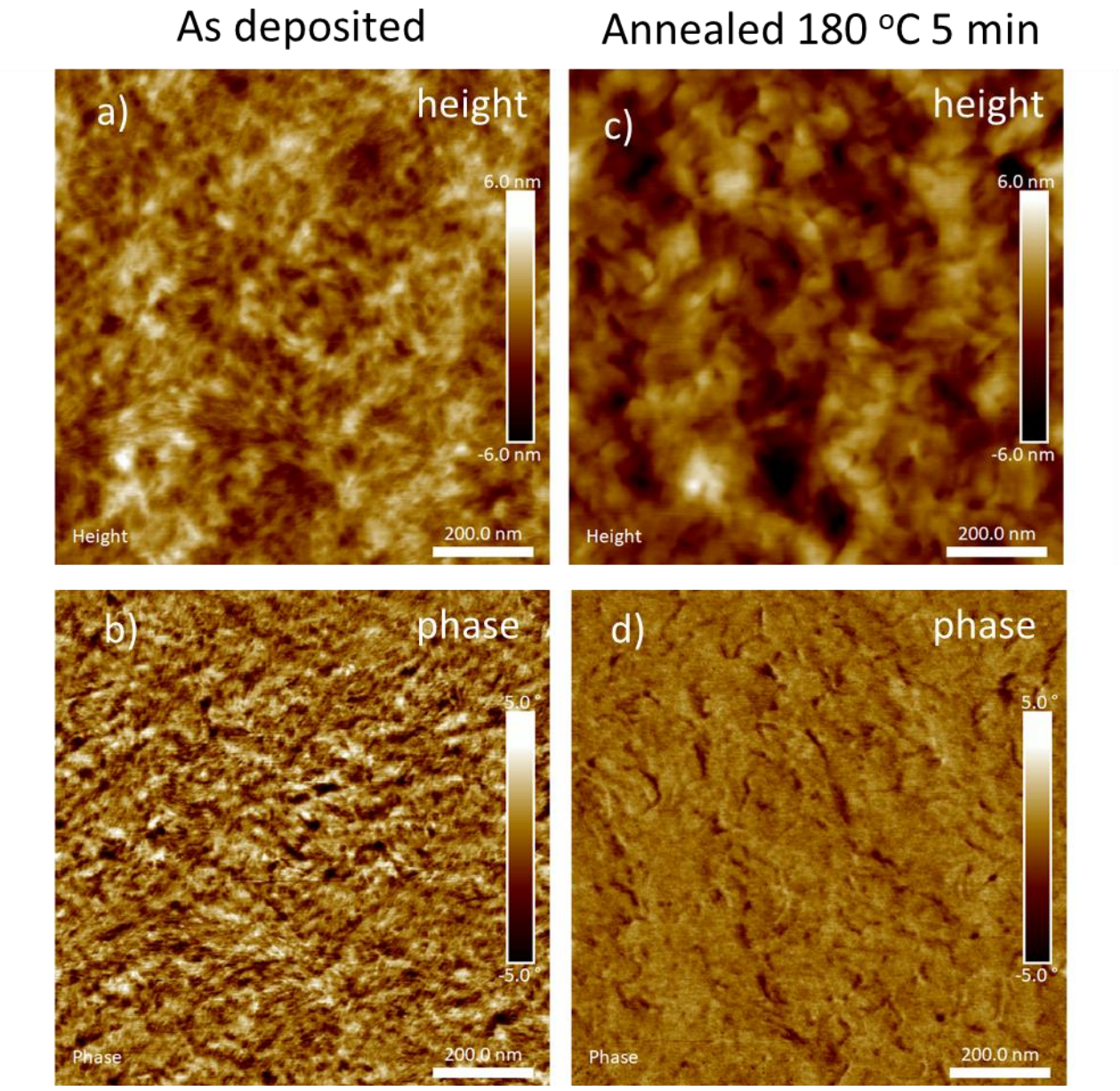

Figure S4: AFM Topography (a and c) and phase (b and d) images for undoped, as-deposited PBTTT film (a, b) and undoped, annealed PBTTT film (c, d). These samples were spin coated onto silicon substrates to enhance the visualization of the morphology (c.f. rough glass substrates).

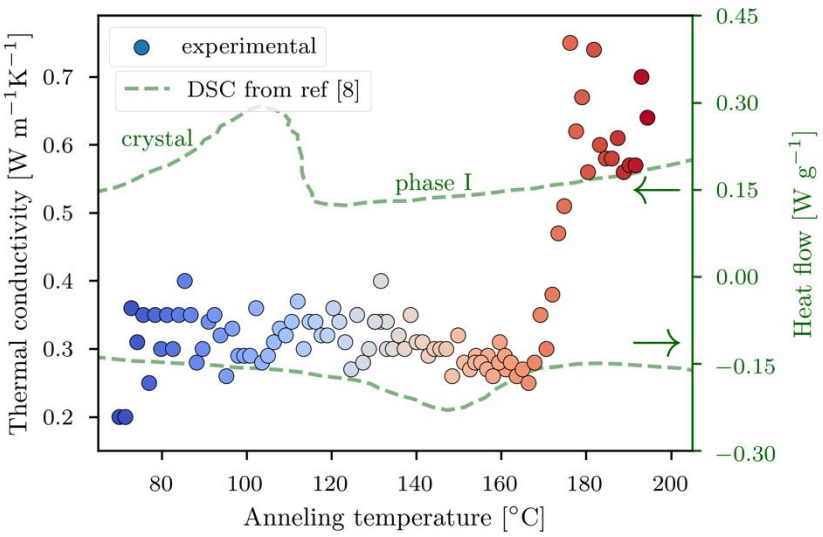

Figure S5. Thermal conductivity as a function of the annealing temperature, and a differential scanning calorimetry (DSC) for PBTTT in the same range of temperature adapted from reference [8]. Data corresponds to sample shown in Figure 1b of the main text.

Figure S5 shows an increase in the thermal conductivity around ~170 ºC. We highlight the increase in thermal conductivity observed in Figure 1b, coincides with the necessary temperature to induce phase transition (crystal → phase I→ crystal thermal cycle). This phase exhibits high levels of order and larger crystalline domains [8]

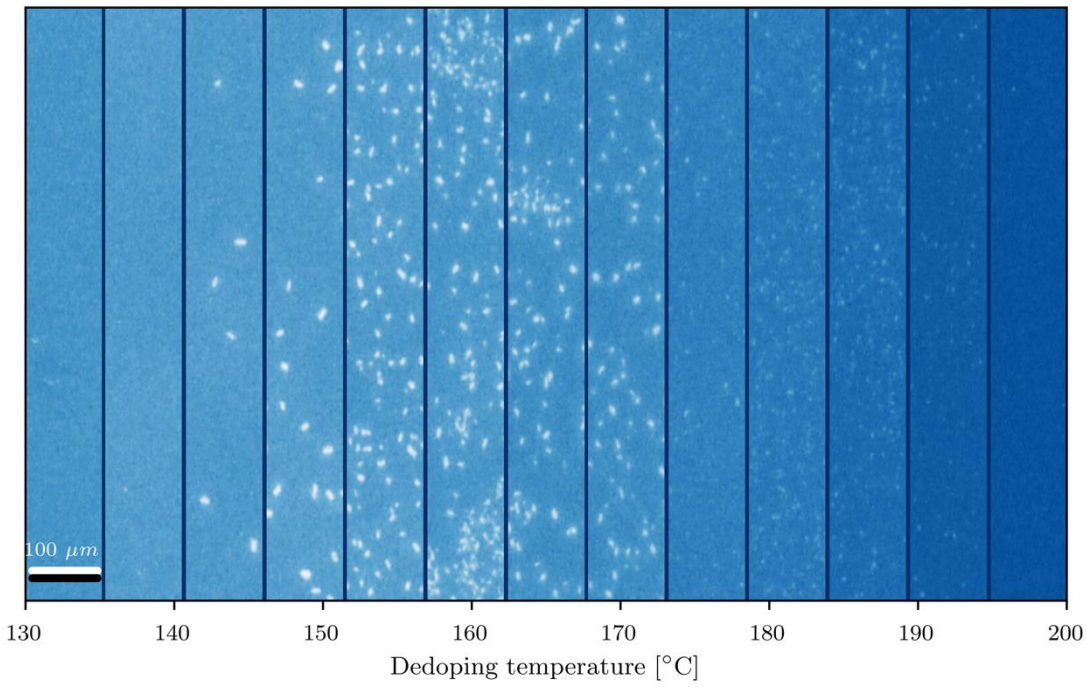

Figure S6: Transmitted-light microscopy for a dedoped film of PBTTT, a pseudo-color was added in order to enhance contrast of the F4TCNQ crystals. White dots correspond to F4TCNQ crystals diffusing out of the PBTTT microstructure and aggregating onto the surface of the polymer film. Bottom scale corresponds dedoping temperature for the experiments depicted in Figure 1d and 1e. Images were taken approximately every 5 mm and thus correspond to a change in a de-doping temperature of approximately 5ºC.

As seen in Figure 2e of the main text, some points in the thermal conductivity between 145 ºC and 170 ºC fall out of the trend. In this work we attribute those points to a high density of F4TCNQ crystals aggregated onto the polymer surface. We point that the model used for fitting the FDTR results contemplates a gold transductor, a polymer film and a glass substrate. Whereas a high density of crystals most likely acts as an additional layer. Thus, giving an average thermal conductivity different than expected.

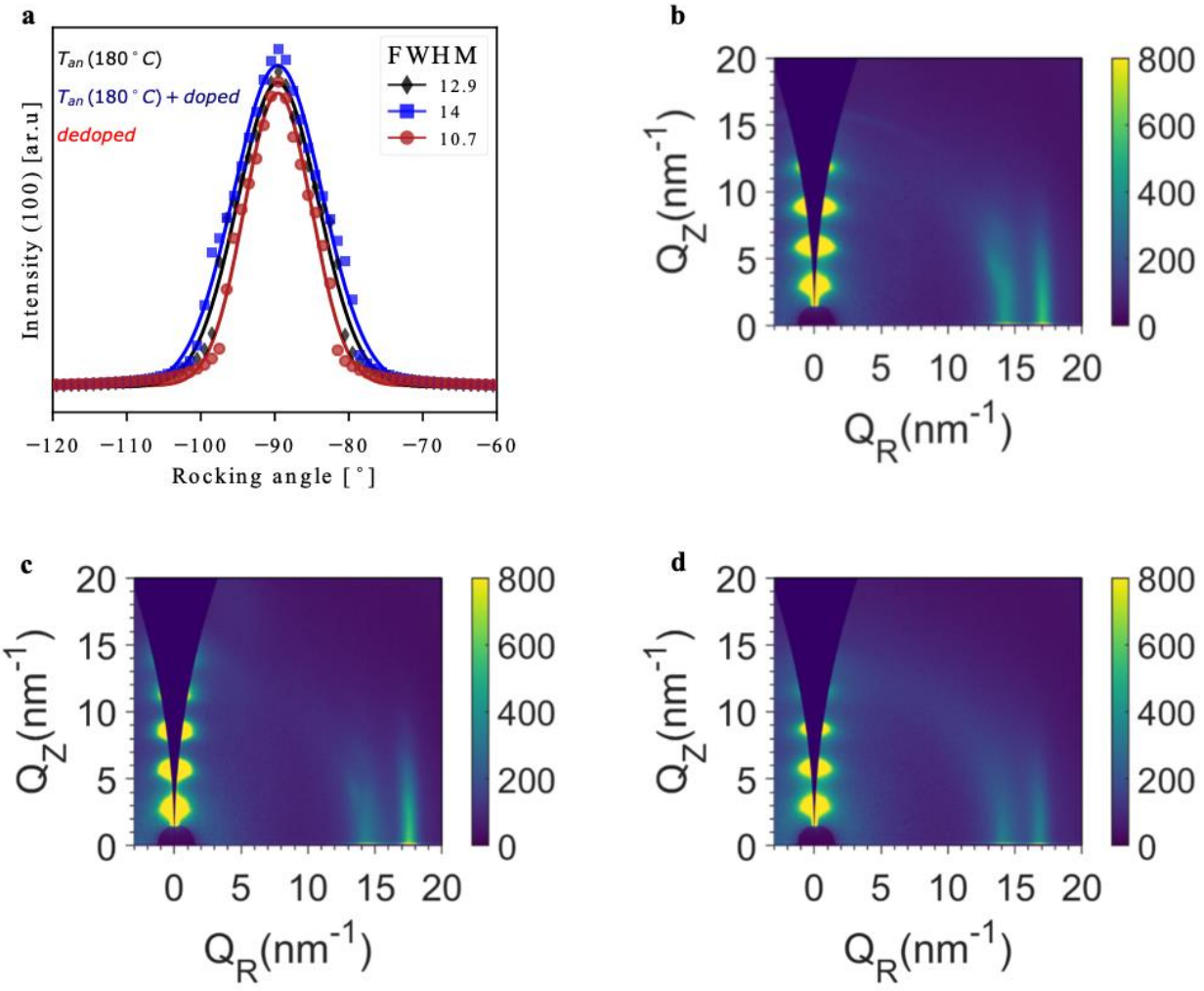

Figure S7: Rocking curves for the (100) reflection depicted in figure 2a. A lower FWHM depicts a larger population of crystals parallel to the substrate. 2D GIWAXS for a) T (180 ºC), b) T (180 ºC + doped), and c) T (180 ºC + dedoped).

Figure S7 demonstrates that dopant induces a relative disorder compared to the pristine sample annealed at 180ºC. On the other hand, the dedoped sample possess an improved orientation compared to the other two, herein attributed to the secondary and more extended annealing process used for dedoping the sample.

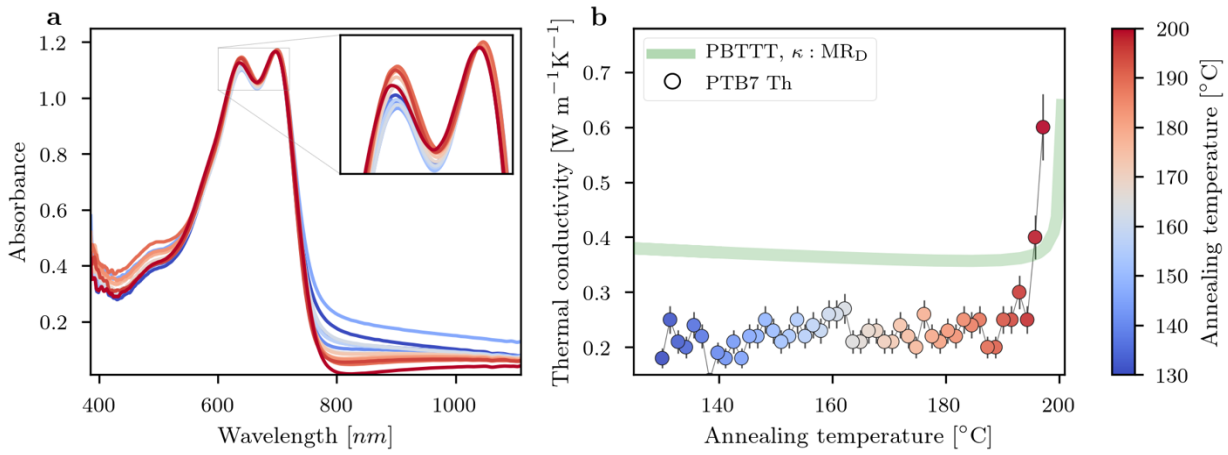

Figure S8: Absorption spectra of PTB7-Th and b) Thermal conductivity for PTB7-Th. This sample was exposed to vapor of F4TCNQ and subsequently annealed in a temperature gradient to remove the dopant. For comparison, green line depicts the effect seen in doped PBTTT and dedoped in the same range of temperatures, as seen in Figure 1e of the main text.

Figure S8 presents an alternative scenario where there is no charge transfer between the polymer and the dopant (PTB7-Th: F4TCNQ), as seen by absent F4TCNQ anion features at 415 nm. This suggest a charge transfer process is not a requirement for the thermal alloy scattering effect seen in Figure 1e of the main text. Neutral molecules could contribute to decrease the lattice thermal conductivity provided that they are dissolved within the polymer matrix, as F4TCNQ crystallites will have a much higher thermal conductivity compared to the polymer, leading to effective thermal conductivities in excess of 5W/mK.[1]

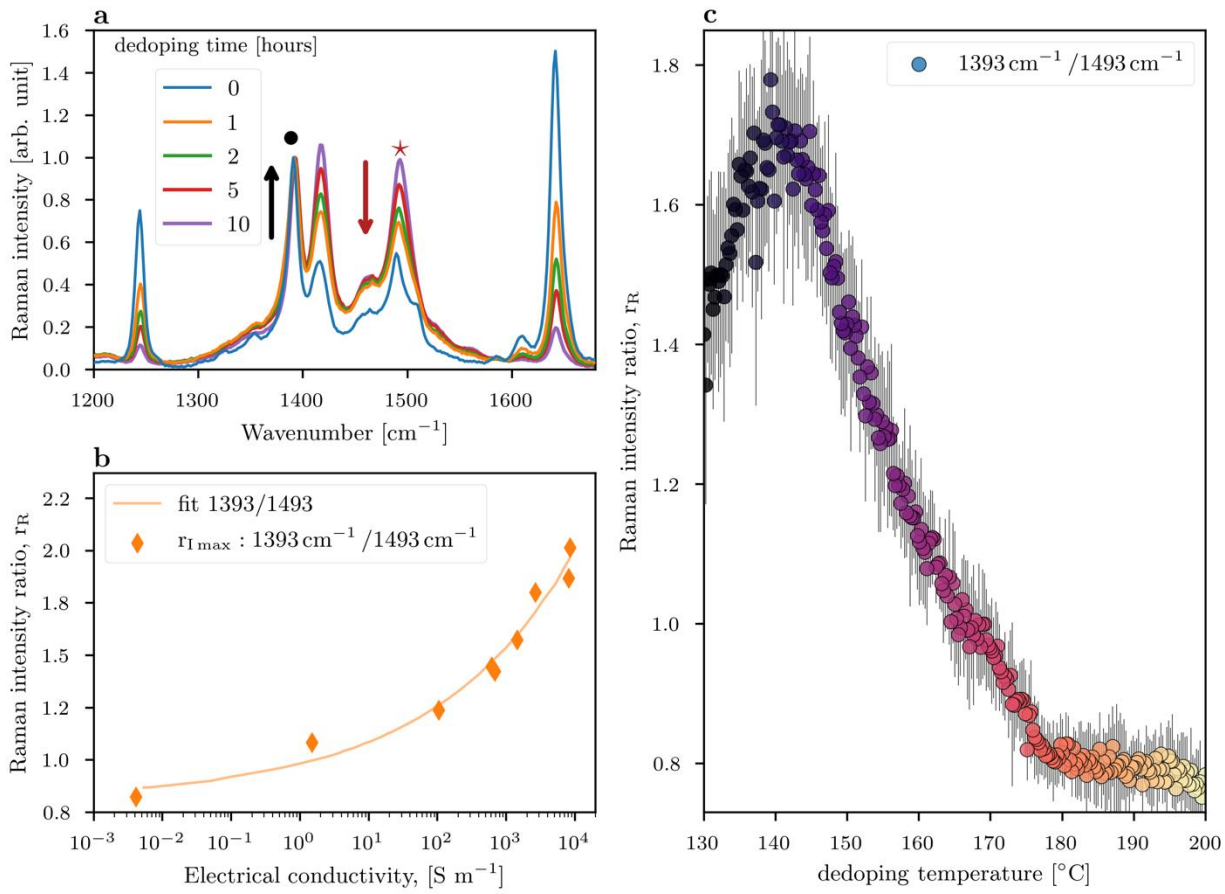

Figure S9: Raman mapping for calculating the electrical conductivity. a) Raman spectra for a homogeneously doped film of PBTTT dedoped at 100ºC at increasing time intervals. b) Ratio of Raman intensities, r_R, for the ~1393 cm^{-1}: ~1493 cm^{-1} peaks as a function of electrical conductivity. c) Raman mapping extracted from the sample shown in Figure 1d of the main text.

Here we show the map of the ratio of Raman intensities for the doped sample presented in Figure 1d of the main text. As shown in Figure S9, by fabricating a calibration curve from homogeneously doped samples, it is possible to make a contactless and local determination of the electrical conductivity. For our experiments, the Raman map in Figure S9c gives us access to an ample range of electrical conductivities as presented in Figure 3 of the main text.

References

(1) Zapata-Arteaga, O.; Dörling, B.; Perevedentsev, A.; Martín, J.; Reparaz, J. S.; Campoy-Quiles, M. Closing the Stability–Performance Gap in Organic Thermoelectrics by Adjusting the Partial to Integer Charge Transfer Ratio. *Macromolecules* **2020**, *53* (2), 609–620.

(2) Schmidt, A. J.; Cheaito, R.; Chiesa, M. A Frequency-Domain Thermoreflectance Method for the Characterization of Thermal Properties. *Rev. Sci. Instrum.* **2009**, *80* (9), 094901.

(3) Vijayakumar, V.; Zaborova, E.; Biniek, L.; Zeng, H.; Herrmann, L.; Carvalho, A.; Boyron, O.; Leclerc, N.; Brinkmann, M. Effect of Alkyl Side Chain Length on Doping Kinetics, Thermopower, and Charge Transport Properties in Highly Oriented F 4 TCNQ-Doped PBTTT Films. *ACS Appl. Mater. Interfaces* **2019**, *11* (5), 4942–4953.

(4) Ma, T.; Dong, B. X.; Grocke, G. L.; Strzalka, J.; Patel, S. N. Leveraging Sequential Doping of Semiconducting Polymers to Enable Functionally Graded Materials for Organic Thermoelectrics. *Macromolecules* **2020**.

(5) Hamidi-Sakr, A.; Biniek, L.; Bantignies, J.-L.; Maurin, D.; Herrmann, L.; Leclerc, N.; Lévêque, P.; Vijayakumar, V.; Zimmermann, N.; Brinkmann, M. A Versatile Method to Fabricate Highly In-Plane Aligned Conducting Polymer Films with Anisotropic Charge Transport and Thermoelectric Properties: The Key Role of Alkyl Side Chain Layers on the Doping Mechanism. *Adv. Funct. Mater.* **2017**, *27* (25), 1700173.

(6) Clark, J.; Chang, J. F.; Spano, F. C.; Friend, R. H.; Silva, C. Determining Exciton Bandwidth and Film Microstructure in Polythiophene Films Using Linear Absorption Spectroscopy. *Appl. Phys. Lett.* **2009**, *94* (16).

(7) Hynynen, J.; Kiefer, D.; Yu, L.; Kroon, R.; Munir, R.; Amassian, A.; Kemerink, M.; Müller, C. Enhanced Electrical Conductivity of Molecularly P-Doped Poly(3-Hexylthiophene) through Understanding the Correlation with Solid-State Order. *Macromolecules* **2017**, *50* (20), 8140–8148.

(8) Delongchamp, D. M.; Kline, R. J.; Jung, Y.; Germack, D. S.; Lin, E. K.; Moad, A. J.; Richter, L. J.; Toney, M. F.; Heeney, M.; Mcculloch, I. Controlling the Orientation of Terraced Nanoscale "Ribbons" of a Poly(Thiophene) Semiconductor. *ACS Nano* **2009**, *3* (4), 780–787.